ISSN 1674-1056
http://cpb.iphy.ac.cn
http://iopscience.iop.org/cpb
中国物理 B
Chinese Physics
中国物理
Chinese Physics B

Broad-band phase retrieval method for transient radial shearing interference using chirp Z transform technique

Fang Xue(薛芳), Ya-Xuan Duan(段亚轩), Xiao-Yi Chen(陈晓义), Ming Li(李铭), Suo-Chao Yuan(袁索超), and Zheng-Shang Da(达争尚)

Citation: Chin. Phys. B, 2021, 30 (**8**): 084209. DOI: 10.1088/1674-1056/abff2f
Journal homepage: http://cpb.iphy.ac.cn; http://iopscience.iop.org/cpb

What follows is a list of articles you may be interested in

Real time high accuracy phase contrast imaging with parallel acquisition speckle tracking

Zhe Hu(胡哲), Wen-Qiang Hua(滑文强), and Jie Wang(王 劼)
Chin. Phys. B, 2021, 30 (**6**): 064201. DOI: 10.1088/1674-1056/abee08

Phase retrieval algorithm for optical information security

Shi-Qing Wang(王诗晴), Xiang-Feng Meng(孟祥锋), Yu-Rong Wang(王玉荣), Yong-Kai Yin(殷永凯), Xiu-Lun Yang(杨修伦)
Chin. Phys. B, 2019, 28 (**8**): 084203. DOI: 10.1088/1674-1056/28/8/084203

Rapid measurement of transmission matrix with the sequential semi-definite programming method

Zhenfeng Zhang(张振峰), Bin Zhang(张彬), Qi Feng(冯祺), Huimei He(何惠梅), Yingchun Ding(丁迎春)
Chin. Phys. B, 2018, 27 (**8**): 084201. DOI: 10.1088/1674-1056/27/8/084201

Application of optical diffraction method in designing phase plates

Ze-Min Lei(雷泽民), Xiao-Yan Sun(孙晓艳), Feng-Nian Lv(吕凤年), Zhen Zhang(张臻), Xing-Qiang Lu(卢兴强)
Chin. Phys. B, 2016, 25 (**11**): 114201. DOI: 10.1088/1674-1056/25/11/114201

Phase-only stereoscopic hologram calculation based on Gerchberg-Saxton iterative algorithm

Xinyi Xia(夏心怡), Jun Xia(夏军)
Chin. Phys. B, 2016, 25 (**9**): 094204. DOI: 10.1088/1674-1056/25/9/094204

Broad-band phase retrieval method for transient radial shearing interference using chirp Z transform technique*

Fang Xue(薛芳)[1,2], Ya-Xuan Duan(段亚轩)[1,†], Xiao-Yi Chen(陈晓义)[1,2], Ming Li[1,2](李铭), Suo-Chao Yuan(袁索超)[1,2], and Zheng-Shang Da(达争尚)[1]

[1] *The Advanced Optical Instrument Research Department, Xi'an Institute of Optics and Precision Mechanics, Chinese Academy of Sciences, Xi'an* 710119, *China*

[2] *University of Chinese Academy of Sciences, Beijing* 100049, *China*

(Received 24 March 2021; revised manuscript received 5 May 2021; accepted manuscript online 8 May 2021)

The transient radial shearing interferometry technique based on fast Fourier transform (FFT) provides a means for the measurement of the wavefront phase of transient light field. However, which factors affect the spatial bandwidth of the wavefront phase measurement of this technology and how to achieve high-precision measurement of the broad-band transient wavefront phase are problems that need to be studied further. To this end, a theoretical model of phase-retrieved bandwidth of radial shearing interferometry is established in this paper. The influence of the spatial carrier frequency and the calculation window on phase-retrieved bandwidth is analyzed, and the optimal carrier frequency and calculation window are obtained. On this basis, a broad-band transient radial shearing interference phase-retrieval method based on chirp Z transform (CZT) is proposed, and the corresponding algorithm is given. Through theoretical simulation, a known phase is used to generate the interferogram and it is retrieved by the traditional method and the proposed method respectively. The residual wavefront RMS of the traditional method is 0.146λ, and it is 0.037λ for the proposed method, which manifests an improvement of accuracy by an order of magnitude. At the same time, different levels of signal-to-noise ratios (SNRs) from 50 dB to 10 dB of the interferogram are simulated, and the RMS of the residual wavefront is from 0.040λ to 0.066λ. In terms of experiments, an experimental verification device based on a phase-only spatial light modulator is built, and the known phase on the modulator is retrieved from the actual interferogram. The RMS of the residual wavefront retrieved through FFT is 0.112λ, and it decreases to 0.035λ through CZT. The experimental results verify the effectiveness of the method proposed in this paper. Furthermore, the method can be used in other types of spatial carrier frequency interference, such as lateral shearing interference, rotational shearing interference, flipping shearing interference, and four-wave shearing interference.

Keywords: radial shearing interference, chirp Z transform (CZT), phase retrieval

PACS: 42.25.Hz, 42.30.Kq, 42.30.Rx **DOI:** 10.1088/1674-1056/abff2f

1. Introduction

Radial shearing interference[1–4] means that the light to be measured is divided into two beams by scaling radially, and then two beams interfere. Compared with traditional interferometry techniques, it achieves high-precision wavefront detection without introducing a high-precision reference wavefront. Therefore, it is widely used in the fields of laser parameter diagnosis,[5,6] human corneal topography[7] and the diagnosis of laser plasma flow field.[8–10] The interferogram obtained by the radial shearing interferometer contains the phase information of the measured wavefront. Phase-shifting interferometry measurement[11–13] and fast Fourier transform (FFT) based on spatial carrier frequency[4,6] are used for phase retrieval. The phase-shifting algorithm needs to collect multiple phase-shifting interferograms in the time domain. Since the interferogram needs to be analyzed at the same time, it cannot meet the requirements of transient wavefront measurement. The FFT only requires calculation of one frame of the interferogram introduced by the spatial carrier frequency, and extracts the first-order level spectrum that restores the measured phase, so it can resist vibration and air disturbance very well. Moreover, the FFT based on radial shearing interferometry does not require the reference light and the phase shift, which provides a means to achieve transient high-precision light field wavefront measurement. However, FFT cannot customize the sampling interval when the spatial sampling interval is small, resulting in under-sampling of the first-order level spectrum, which makes the accuracy of phase retrieval low. To solve this problem, the FFT method with zero padding and dimensional expansion can be used to customize the frequency domain sampling interval.[14] However, this method increases the number of samples, and zero padding will cause a ringing phenomenon on the retrieved phase. Which factors affect the spatial bandwidth of the wavefront phase measurement of this technology and how to achieve high-precision measurement of the broad-band transient wavefront phase are problems that need to be studied further.

In order to achieve high-precision measurement of

*Project supported by the National Natural Science Foundation of China (Grant No. 61705254) and the Key Research and Development Program of Shaanxi Province of China (Grant No. 2020GY-114).

†Corresponding author. E-mail: duanyaxuan@opt.ac.cn

© 2021 Chinese Physical Society and IOP Publishing Ltd

the high-frequency wavefront, a broad-band phase retrieval method for transient radial shearing interference using the chirp Z transform (CZT) is proposed in this paper.[14] The remaining parts of this paper are organized as follows: In Section 2, the basic principle of phase retrieval for the transient radial shearing interference is introduced at the beginning. Then a bandwidth theoretical model based on the spatial carrier frequency for the phase retrieval of radial shearing interference is established and the best carrier frequency and calculation window are deduced. Finally, the CZT algorithm is introduced. Section 3 gives the corresponding phase retrieval algorithm based on CZT. Sections 4 and 5 are the simulation and experimental verification of the proposed method, respectively. The conclusion is drawn in Section 6.

2. Theory

2.1. Transient phase retrieval of radial shearing interference

The annular radial shearing interference system[14,15] is taken as an example, and the structure chart is shown in Fig. 1. It is mainly composed of a splitting prism BS1, two plane mirrors M1 and M2, a telescope system with lens L1 and L2, and an image acquisition system CCD.

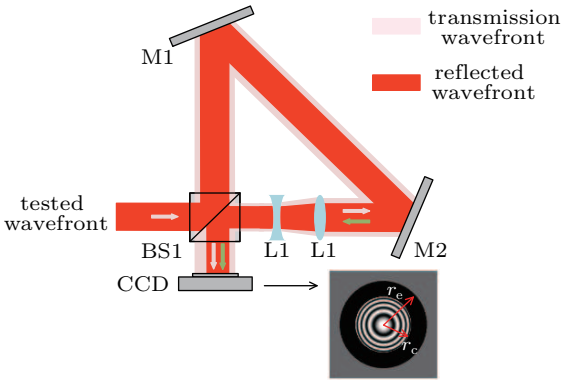


Fig. 1. Schematic diagram of annular radial shearing interference system. r_e and r_c represent the radial radius of the expanded light field and the reduced light field.

The light field to be measured is divided into the reduced light field and the expanded light field of which the wavefront aberration stays unchanged during field transportation, and the shearing ratio is $\beta = r_c/r_e$. Then, the shearing wavefront is obtained when the expanded light field and the reduced light field interfere at the CCD, so the spatial carrier frequency method[6,16] is used by tilting BS1 at a slight angle. The expression of the intensity of the radial shearing interference fringe is

$$\begin{aligned} I(x,y) &= I_0(x,y) \\ &\quad + a(x,y)\cos[2\pi f_{0x}x + 2\pi f_{0y}y + kW_{\mathrm{OPD}}(x,y)], \end{aligned} \tag{1}$$

where $I_0(x,y)$ is the background information, $a(x,y)$ is the fringe modulation, k is the wave number (mm^{-1}), $W_{\mathrm{OPD}}(x,y)$ is the shearing wavefront (mm), f_{0x} and f_{0y} denote carrier frequency on x and y (mm^{-1}), respectively. They satisfy

$$f_0 = f_{0x} = f_{0y} = \frac{\sin\gamma}{\lambda}, \tag{2}$$

where γ is the slight angle of the BS1, and λ is the wavelength. Equation (1) can be simplified to

$$\begin{aligned} I(x,y) &= I_0(x,y) + b(x,y)\exp[\mathrm{i}2\pi(f_x x + f_y y)] \\ &\quad + b^*(x,y)\exp[-\mathrm{i}2\pi(f_x x + f_y y)], \end{aligned} \tag{3}$$

where $b(x,y) = \frac{1}{2}a(x,y)\exp[\mathrm{i}kW_{\mathrm{OPD}}(x,y)]$.

The Fourier transform of Eq. (3) obtains the interference field spectrum as

$$\begin{aligned} I(f_x,f_y) &= I_0(f_x,f_y) + B(f_x - f_{0x}, f_y - f_{0y}) \\ &\quad + B^*(f_x + f_{0x}, f_y + f_{0y}), \end{aligned} \tag{4}$$

where $I(f_x,f_y)$, $I_0(f_x,f_y)$, $B(f_x - f_{0x}, f_y - f_{0y})$ and $B^*(f_x + f_{0x}, f_y + f_{0y})$ respectively represent the Fourier spectrum corresponding to each term in Eq. (3). As shown in Fig. 2, $B(f_x - f_{0x}, f_y - f_{0y})$ is the first-order spectrum. The window size is generally half of the distance between the zero-order spectrum and the first-order spectrum in the traditional FFT. If $B(f_x - f_{0x}, f_y - f_{0y})$ is further shifted to the origin, $B(f_x,f_y)$ is obtained. The inverse Fourier transform of $B(f_x,f_y)$ is

$$b(x,y) = \mathrm{F}^{-1}\{B(f_x,f_y)\}, \tag{5}$$

where F^{-1} represents inverse Fourier transform. According to Eq. (5) the process of eliminating tilt is

$$W_{\mathrm{OPD}}(x,y) = \arctan\left\{\frac{\mathrm{Im}[b(x,y)]}{\mathrm{Re}[b(x,y)]}\right\}, \tag{6}$$

where $\mathrm{Re}[b(x,y)]$ and $\mathrm{Im}[b(x,y)]$ respectively denote the real and imaginary parts of $b(x,y)$.

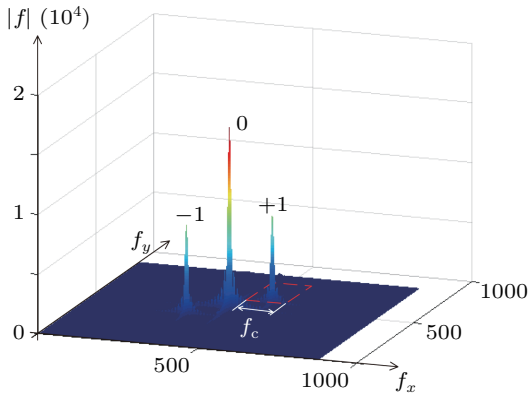


Fig. 2. Radial shearing interference spectrum. f_c is the retrieved bandwidth of the first-order spectrum.

The true first-order spectrum is obtained, which is wrapped by the wrapping operator[17,18] in Eq. (7), namely,

$$U_{\mathrm{OPD}i,j} = W_{\mathrm{OPD}i,j} + 2\pi k_{i,j}, \quad k \in Z, \tag{7}$$

where $W_{\mathrm{OPD}i,j}$ is the wrapped phase, $U_{\mathrm{OPD}i,j}$ is the true phase, $k_{i,j}$ is an integer, $0 \le i \le M-1$ and $0 \le j \le N-1$, and M and

N are the number of sampling points. The shearing wavefront after the phase unwrapping is as follows:

$$U_{\mathrm{OPD}}(x/s,y/s)=U(x/s,y/s)-U(sx,sy), \tag{8}$$

where s is the reduction ratio, $\beta=s^2$. The original field distribution is restored through an iterative algorithm,[16] and by multiplying x and y by s respectively in Eq. (8) to obtain

$$U_{\mathrm{OPD}}(x,y)=U(x,y)-U\left(s^2x,s^2y\right). \tag{9}$$

After q iterations, adding all equations and simplifying, we obtain

$$\begin{aligned}&\sum_{i=-1}^{q}U_{\mathrm{OPD}}\left(s^ix,s^iy\right)+U\left(s^{q+1}x,s^{q+1}y\right)+U\left(s^{q+2}x,s^{q+2}y\right)\\&=U(x,y)+U(x/s,y/s),\end{aligned} \tag{10}$$

where $U\left(s^{q+1}x,s^{q+1}y\right)+U\left(s^{q+2}x,s^{q+2}y\right)$ is the error of measurement. The error approaches zero after q iterations, and $U(x,y)+U(x/s,y/s)$ is obtained. Similarly, we multiply x and y by β respectively in Eq. (8) to obtain

$$U_{\mathrm{OPD}}(sx,sy)=U(sx,sy)-U\left(s^3x,s^3y\right). \tag{11}$$

After q iterations, $U(x/s,y/s)$ is obtained in the same way as above, and $U(x,y)$ can be obtained from the difference between the two results.

2.2. Bandwidth of phase retrieval

In order to extract the information of the first-order spectrum, the theoretical model of the optimal carrier frequency and the best calculation window for phase retrieval is analyzed. The maximum bandwidth $f_{\max}$ of the frequency spectrum of the radial shearing interference field satisfies

$$f_{\max}=\frac{1}{2\Delta d}, \tag{12}$$

where Δd denotes the spatial sampling interval. The selected window width D_{d} satisfies

$$D_{\mathrm{d}}=\begin{cases}\frac{M}{f_{\max}}(f_0-f_{\mathrm{b}}), & f_{\mathrm{b}}<f_0\le\frac{1}{2}(f_{\max}+f_{\mathrm{b}}),\\ M\left(1-\frac{f_0}{f_{\max}}\right), & \frac{1}{2}(f_{\max}+f_{\mathrm{b}})<f_{\mathrm{b}}<f_{\max},\end{cases} \tag{13}$$

where f_{b} is the cut-off frequency of the zero-order spectrum. Therefore, the bandwidth f_{c} for retrieving the measured phase information is

$$\begin{aligned}f_{\mathrm{c}}&=\frac{2D_{\mathrm{d}}\cdot f_{\max}}{M}\\&=\begin{cases}2(f_0-f_{\mathrm{b}}), & f_{\mathrm{b}}<f_0\le\frac{1}{2}(f_{\max}+f_{\mathrm{b}}),\\ 2(f_{\max}-f_0), & \frac{1}{2}(f_{\max}+f_{\mathrm{b}})<f_0<f_{\max}.\end{cases}\end{aligned} \tag{14}$$

Then, in light of the Nyquist sampling law, the sampling frequency is greater than twice the highest frequency of the signal,

$$f_{\max}\ge 2\left(f_0+\frac{f_{\mathrm{c}}}{2}\right). \tag{15}$$

Substituting it into Eq. (14), the acceptable range of carrier frequency is

$$f_0\in\left(f_{\mathrm{b}},\ \frac{1}{4}f_{\max}+\frac{1}{2}f_{\mathrm{b}}\right]. \tag{16}$$

As shown in Fig. 3, when the carrier frequency is $f_{\mathrm{opt}}=\frac{1}{4}f_{\max}+\frac{1}{2}f_{\mathrm{b}}$, the bandwidth of the retrieved phase is most suitable, namely,

$$f_{\mathrm{c,max}}=\frac{1}{2}f_{\max}-f_{\mathrm{b}}. \tag{17}$$

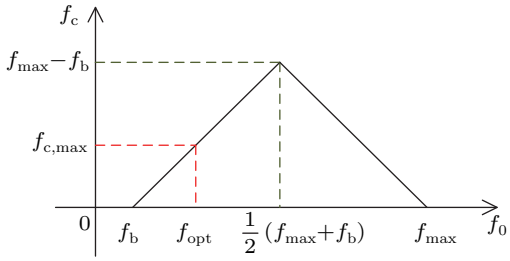


Fig. 3. The relationship diagram between phase retrieved bandwidth f_{c} and carrier frequency f_0. The frequency (red line) denotes the optimal carrier frequency and the optimal bandwidth.

The determination of the optimal calculation window depends on the cut-off frequency f_{b} of the zero-order spectrum. FFT cannot customize the sampling interval, and the spectrum determined by carrier frequency is often prone to undersampling, which makes the error about the window selection of the first-order spectrum larger, resulting in a smaller bandwidth.

2.3. Chirp Z transform

In order to obtain the cut-off frequency of the zero-order spectrum accurately, the CZT[19,20] is introduced, which reduces the sampling interval of the frequency domain. Supposing the input function is $f(x)$, then its CZT expression is

$$\begin{aligned}&F_\alpha(m)=\sum_{n=-N/2}^{N/2}f(n)\exp\left(-\mathrm{i}2\pi\frac{\alpha mn}{N}\right),\\&\left\{\begin{array}{l}m\in(-M/2,M/2-1]\\ n\in(-N/2,N/2-1]\end{array}\right\},\end{aligned} \tag{18}$$

where α is the scaling factor, and it represents the ratio of the number of sampling points in the frequency domain for CZT and FFT. It can be sorted into

$$\begin{aligned}F_\alpha(m)&=\exp\left(-\mathrm{i}\pi\frac{\alpha m^2}{N}\right)\sum_{n=-N/2}^{N/2}f(n)\exp\left(-\mathrm{i}\pi\frac{\alpha n^2}{N}\right)\\&\quad\times\exp\left(\mathrm{i}\pi\frac{\alpha(n-m)^2}{N}\right)\\&=\exp\left(-\mathrm{i}\pi\frac{\alpha m^2}{N}\right)\cdot\mathrm{F}^{-1}\left\{\mathrm{F}\{p(n)\}\times\mathrm{F}\{q(n)\}\right\},\end{aligned} \tag{19}$$

where $p(n)=f(n)\exp\left(-\mathrm{i}\pi\frac{\alpha n^2}{N}\right)$ and $q(n)=\exp\left(\mathrm{i}\pi\frac{\alpha n^2}{N}\right)$.

The calculation process can be broken down into two multiplications and one convolution as shown in Fig. 4. When

the scaling factor takes a negative value, CZT inverse transformation can be performed.

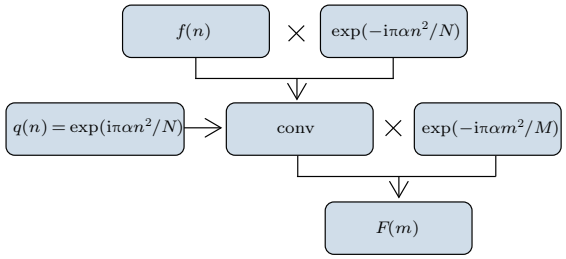


Fig. 4. CZT transformation flowchart.

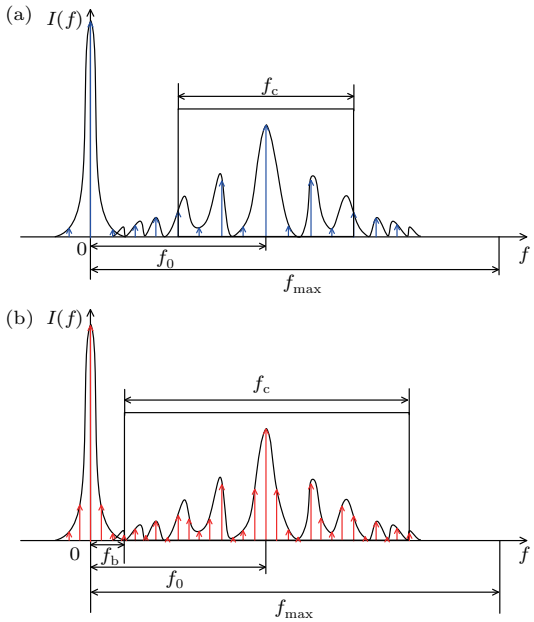


Fig. 5. Spectrogram of FFT and CZT. (a) FFT spectrogram; the blue arrow indicates the sampling point. (b) CZT spectrogram; the red arrow indicates the sampling point.

Since the discrete Fourier domain convolution is a circular convolution, it needs to be converted into a linear convolution by zero padding. In order to avoid aliasing, we add zeros around the sequence $p(n)$ to make the sequence length greater than or equal to $M+N-1$.[19,20] According to the above steps, CZT can be realized. The CZT algorithm is flexible, and the number of samples in the frequency domain can be adjusted by changing the scaling factor, so it can be used to reduce the sampling interval of frequency domain to increase the bandwidth of the phase. Figure 5 compares FFT and CZT that only consider a one-dimensional spectrum for the convenience of analysis.

It can be seen from Fig. 5 that CZT has a finer spectrum compared to FFT. Based on the phase-retrieval model, the bandwidth is significantly larger than that of FFT.

3. Phase-retrieval algorithm

The phase-retrieval algorithm flow of transient radial shearing interference based on CZT is shown in Fig. 6. It mainly consists of four steps: (i) determine the cut-off frequency of the zero-order spectrum; (ii) determine the optimal spatial carrier frequency and bandwidth and reacquire the radial shearing interferogram under the optimal carrier frequency; (iii) perform CZT transformation and extract the first-order spectrum with the optimal bandwidth; (iv) phase unwrapping to get the shearing phase and shearing phase multiple iterations.

Step 1 The carrier frequency is entered and the radial shearing interferogram is obtained at the CCD by Eq. (2). The sampling point is 200×200. The CCD sampling interval is $\Delta d = 0.0074$ mm.

The coordinates (f_{x0}, f_{y0}) and (f_{x1}, f_{y1}) of the zero-order and first-order spectrum are determined after CZT transformation. The coordinates (f_{bx}, f_{by}) are determined through the minimum calibration algorithm that selected the minimum

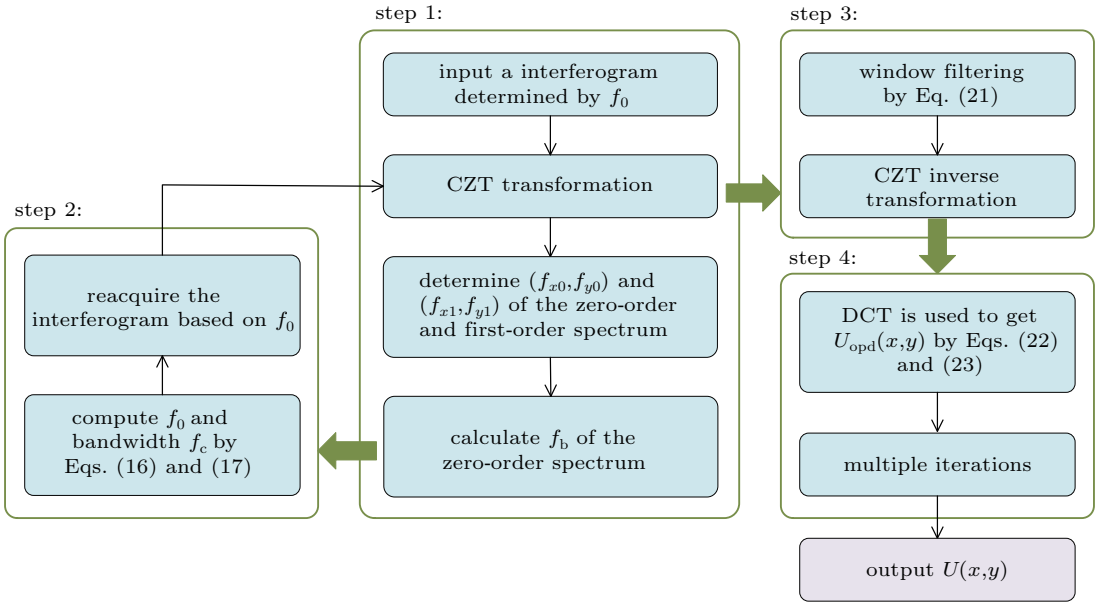


Fig. 6. Phase-retrieval flowchart of radial shearing interference.

value in Eq. (20), and the value is considered as the cut-off frequency f_{b} of the zero-order spectrum.

$$\begin{aligned} I\left(f_{\mathrm{b}x}, f_{\mathrm{b}y}\right) &= \min\left\{I\left(f_{x0}, f_{y0}\right), I\left(f_{x0+1}, f_{y0+1}\right), \ldots, \right. \\ &\quad \left. I\left(f_{x1-1}, f_{y1-1}\right), I\left(f_{x1}, f_{y1}\right)\right\}, \\ f_{\mathrm{b}} &= f_{\mathrm{b}x} = f_{\mathrm{b}y}. \end{aligned} \tag{20}$$

Step 2 The optimal carrier frequency f_0 and the bandwidth f_{c} are obtained precisely by Eqs. (16) and (17).

The slight angle γ at which the optimal carrier frequency is determined by Eq. (2), and the radial shearing interferogram is reacquired by Eq. (1).

Step 3 After CZT transformation, the window function is designed to extract first-order spectrum, namely,

$$\mathrm{Wind}(f_x, f_y) = \begin{cases} \frac{M^2}{f_{\max}^2}\left(f_x - f_{\mathrm{b}}\right)\cdot\left(f_y - f_{\mathrm{b}}\right), & f_{\mathrm{b}} < f_x,\ \ f_y \le \frac{1}{2}\left(f_{\max} + f_{\mathrm{b}}\right), \\ \frac{M^2}{f_{\max}^2}\left(f_{\max} - f_x\right)\cdot\left(f_{\max} - f_y\right), & \frac{1}{2}\left(f_{\max} + f_{\mathrm{b}}\right) < f_x,\ \ f_y < f_{\max}. \end{cases} \tag{21}$$

More phase information is retrieved based on the optimal bandwidth in the first-order spectrum after the CZT inverse transformation.

Step 4 The processing to eliminate tilt is performed by Eq. (6), and the discrete cosine transform (DCT) algorithm[21] is used to carry out the least squares phase unwrapping. By calculating the least second-order norm of the phase gradient error between the measured phase and the wrapped phase, the approximate value of the phase to be measured is obtained as[22]

$$\begin{aligned} \rho_{i,j} &= \sum_{i=0}^{M-2}\sum_{j=0}^{N-1}\left(U_{\mathrm{OPD}i+1,j} - U_{\mathrm{OPD}i,j} - \Delta_{i,j}^{x}\right)^2 \\ &\quad + \sum_{i=0}^{M-1}\sum_{j=0}^{N-2}\left(U_{\mathrm{OPD}i,j+1} - U_{\mathrm{OPD}i,j} - \Delta_{i,j}^{y}\right)^2, \end{aligned} \tag{22}$$

where $\Delta_{i,j}^{x}$ and $\Delta_{i,j}^{y}$ denote the phase difference term from the wrapped phase in the horizontal and the vertical direction.

Solving Eq. (22) is equivalent to solving the Poisson equation with the Neumann boundary and the DCT. The cosine transform coefficient can be obtained by Eq. (22), and the expected solution equation is expanded according to the coefficient[22]

$$\begin{aligned} U_{\mathrm{OPD}i,j} &= \frac{1}{MN}\sum_{m=0}^{M-1}\sum_{n=0}^{N-1} c\left(m,n\right)\hat{\rho}_{m,n}\cos\left[\frac{\pi}{2M}m\left(2i+1\right)\right] \\ &\quad \times\cos\left[\frac{\pi}{2N}n\left(2j+1\right)\right], \end{aligned} \tag{23}$$

where $c\left(m,n\right)$ is the Neumann boundary condition, and $\hat{\rho}_{m,n}$ is the DCT transform form of $\rho_{i,j}$. Then, the shearing phase is obtained by Eq. (23). Multiple iterations of Eqs. (9) and (11) are performed to obtain the measured phase.

4. Simulation and analysis

In this paper, a typical binary wavefront[6] is used as the phase distribution of the source plane, as shown in Figs. 7(a) and 7(b) denotes the amplitude of source plane. Figure 7(c) is the shearing interferogram generated by the radial shearing interference system.

The carrier frequency is artificially set to 12 mm^{-1} and the shearing ratio is 0.64. Next, we perform phase retrieval according to the algorithm flow in Section 3 to compare the accuracy between the proposed method and traditional FFT. As shown in Fig. 8, Figures 8(a) and 8(b) are the retrieved result and residual wavefront with FFT, and the residual RMS is 0.146λ; the retrieved results and residuals with different scaling factors by the proposed method are shown in Figs. 8(c)–8(j). The RMS values of the residual wavefront are 0.068λ ($\alpha = 2$); 0.041λ ($\alpha = 4$); 0.043λ ($\alpha = 6$); 0.041λ ($\alpha = 8$). It can be concluded that the accuracy of the proposed method is an order of magnitude higher than that of FFT.

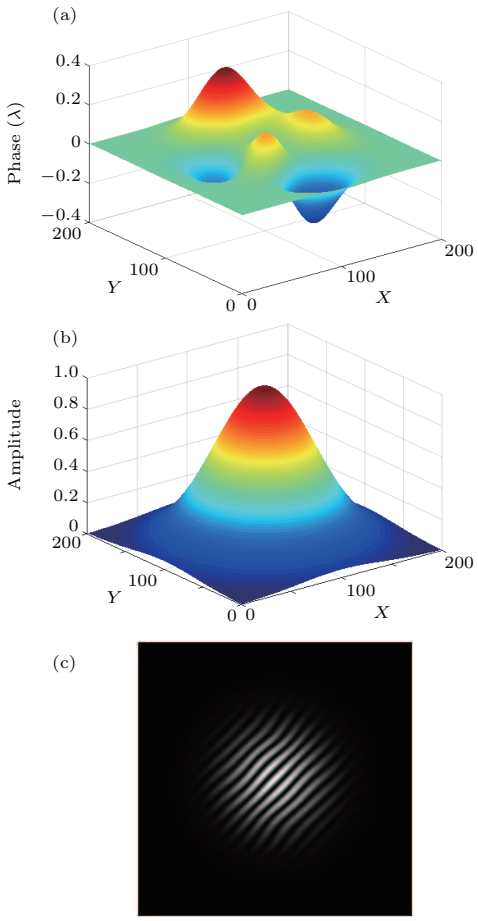


Fig. 7. Ideal wavefront and corresponding ideal interference fringes: (a) denotes the phase distribution with large distortion, here the PV is 0.61λ; (b) represents the Gaussian distribution of which the amplitude is 1; (c) represents the transient radial shearing interferogram, here the wavelength is 635 nm.

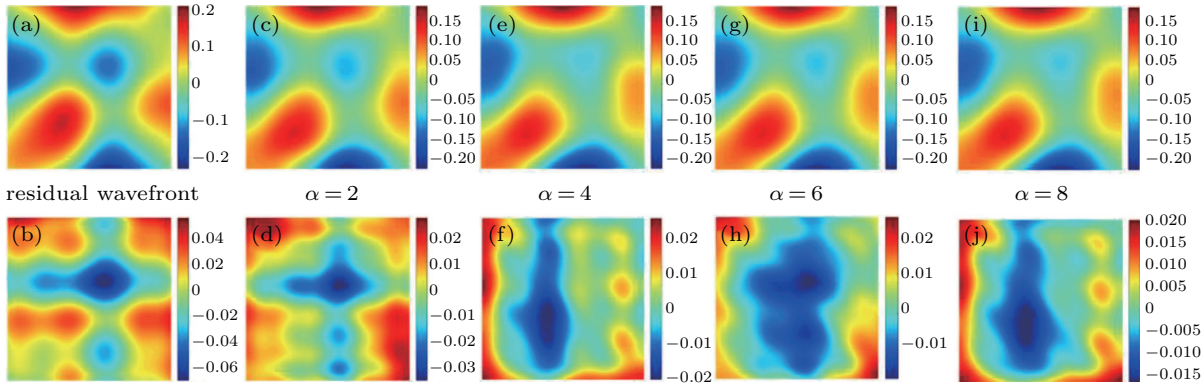


Fig. 8. The retrieved results and residual wavefront: (a), (b) FFT; (c), (d) the proposed method with $\alpha = 2$; (e), (f) the proposed method with $\alpha = 4$; (g), (h) the proposed method with $\alpha = 6$; (i), (j) the proposed method with $\alpha = 8$.

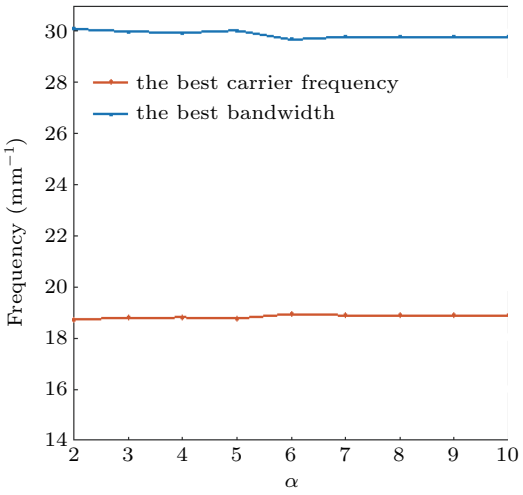


Fig. 9. The optimal carrier frequency (red line) and bandwidth (blue line) with different scaling factors.

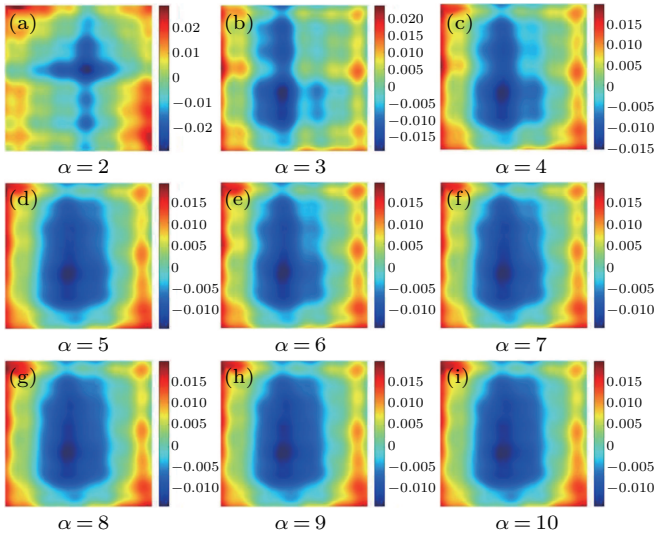


Fig. 10. The residual wavefront based on the optimal carrier frequency and bandwidth with different scaling factors.

The bandwidth of traditional FFT is 12 mm^{-1}. According to the bandwidth of the phase-retrieval model in this paper, the optimal carrier frequency and bandwidth with different scaling factors are shown in Fig. 9, respectively: $f_{\text{opt}} = 18.738$ mm^{-1}, $f_{\text{c,max}} = 30.092$ mm^{-1} (α=2); $f_{\text{opt}} = 18.812$ mm^{-1}, $f_{\text{c,max}} = 29.944$ mm^{-1} (α=4); $f_{\text{opt}} = 18.945$ mm^{-1}, $f_{\text{c,max}} = 29.679$ mm^{-1} (α=6); $f_{\text{opt}} = 18.892$ mm^{-1}, $f_{\text{c,max}} = 29.784$ mm^{-1} (α=8). It can be concluded that the bandwidth of the proposed method is more than twice that of traditional FFT as shown in Fig. 9.

The radial shearing interferogram is reacquired according to the optimal carrier frequency with different scaling factors in Fig. 9, and the residual wavefronts by the proposed method in the paper are shown in Fig. 10. The RMS values of the residuals are: 0.058λ (α=2); 0.040λ (α=3); 0.037λ (α=4); 0.037λ (α=5); 0.037λ (α= 6); 0.037λ (α= 7); 0.038λ (α= 8); 0.038λ (α= 9); 0.038λ (α= 10), as shown in Fig. 11.

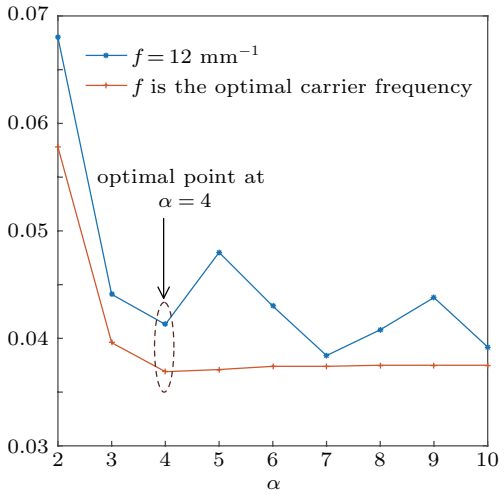


Fig. 11. The comparison of the residual RMS based on the initial carrier frequency (blue line) and the optimal carrier frequency (red line). The dashed line represents the optimal value in both cases.

It can be seen from Fig. 11 that the residual RMS of phase retrieval based on the optimal carrier frequency is smaller than that of phase retrieval based on the initial carrier frequency with different scaling factors. For the proposed method, the larger the scaling factor α, the smaller the residual RMS of phase retrieval; when the scaling factor is 4, the residual RMS is reduced by 36.26% compared with the scaling factor of 2; when α is greater than 4, the maximum change of the residual RMS of phase retrieval is 0.001λ. As the scaling factor increases, the calculation complexity of CZT becomes higher.

In order to balance the accuracy of phase retrieval and calculation efficiency, the scaling factor is recommended to be 4.

In order to verify the noise robustness of the proposed method, Gaussian noise with different signal-to-noise ratio (50 dB to 10 dB) is added to the radial shearing interferogram. The results of phase retrieval by the proposed method are shown in Fig. 12. The RMS values of phase retrieval corresponding to different SNRs are 0.066λ (10 dB), 0.048λ (20 dB), 0.041λ (30 dB), 0.040λ (40 dB), 0.041λ (50 dB), respectively. Results show that the greater the noise, the worse the accuracy of phase retrieval, but it is still better than traditional FFT. It proves the robustness of the broad-band phase retrieval method based on CZT.

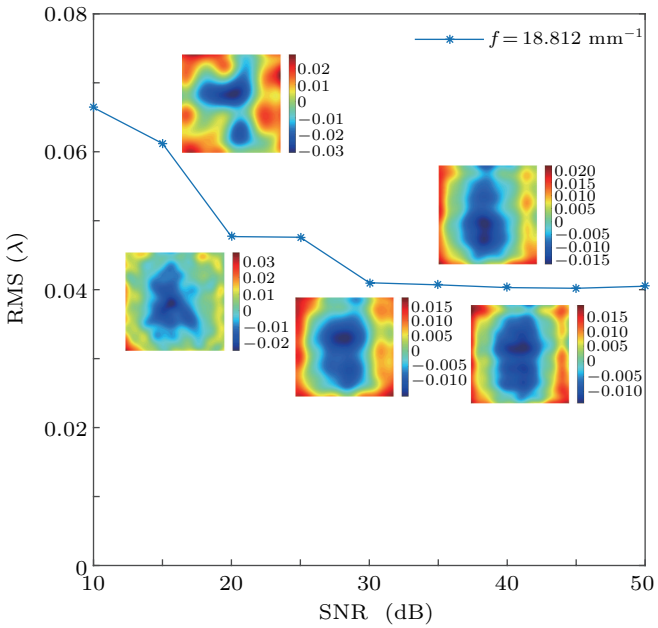


Fig. 12. The comparison of RMS of residual wavefront with different SNRs. The best carrier frequency is 18.812 mm^{-1}; the scaling factor is 4; and the RMS values corresponding to different SNRs are 0.066λ, 0.048λ, 0.041λ, 0.040λ, 0.041λ, respectively.

5. Experiment

The experimental setup is shown in Fig. 13 to verify the broad-band phase retrieval method for transient radial shearing interference using chirp Z transform technique. The laser of wavelength $\lambda = 635$ nm is collimated by the collimating lens and incident on the phase-only spatial light modulator where a known phase is added to the beam through the polarizer. Then, the modulated beam is split by the splitting prism, the transmitted beam and the reflected beam are reflected by the mirrors and passed in forward and reverse directions at the beam expansion system to achieve zooming, and finally the interferogram is obtained by CCD. The parameters in the experimental installation are shown in Table 1.

The phase diagram is shown in Fig. 14(a). The radial shearing interferogram is shown in Fig. 14(b). Figure 15 shows the comparison of retrieved results based on FFT and the proposed method.

Table 1. The parameters of experimental installation.

Device	Technical parameters
Fiber-optic laser	pigtail core diameter 6.2 μm; wavelength 635 nm
Splitting prism BS1	split ratio 50:50
Collimating lens	focal length 100 mm
polarizer	the clear aperture Φ 15 mm; the extinction ratio: less than 5×10^{-6}
Phase-only liquid crystal spatial light modulator	1024×1272; pixel size 12.5 μm; system wavefront error $1/20\lambda$; phase modulation stability 4%
Telescope system	Beam expansion ratio 1.56
CCD detector	2048×2048; pixel size 7.4 μm; 12 bit

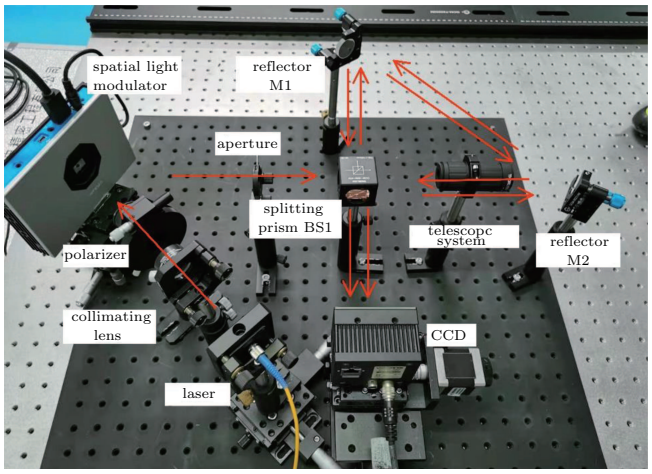


Fig. 13. Annular radial shearing interference verification experimental installation based on the phase-only spatial light modulator.

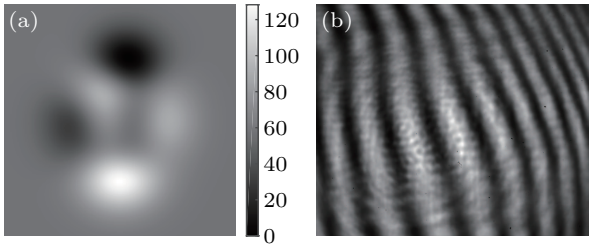


Fig. 14. (a) Phase diagram loaded on the spatial light modulator; here the PV is 0.61λ. (b) Radial shearing interferogram.

Compared with FFT, the bandwidth of the proposed method is increased by 1.8 times, and the window contains more high-frequency information. The phase retrieval of the light field with the known phase modulation is performed through the traditional FFT-based phase retrieval method and the proposed method in this paper, respectively. The retrieved results and the residual results are shown in Fig. 16. For the proposed method, the best parameters are obtained according to the algorithm proposed in Section 3 and the theoretical simulation analysis. The carrier frequency is 18.812 mm^{-1}, the phase retrieved bandwidth is 29.949 mm^{-1}, and the scaling factor is 4. The residual RMS of phase retrieval is 0.112λ through traditional FFT, and the RMS by the proposed method is 0.035λ, which manifests an improvement of accuracy by

an order of magnitude. The experimental results are basically consistent with the theoretical simulation results.

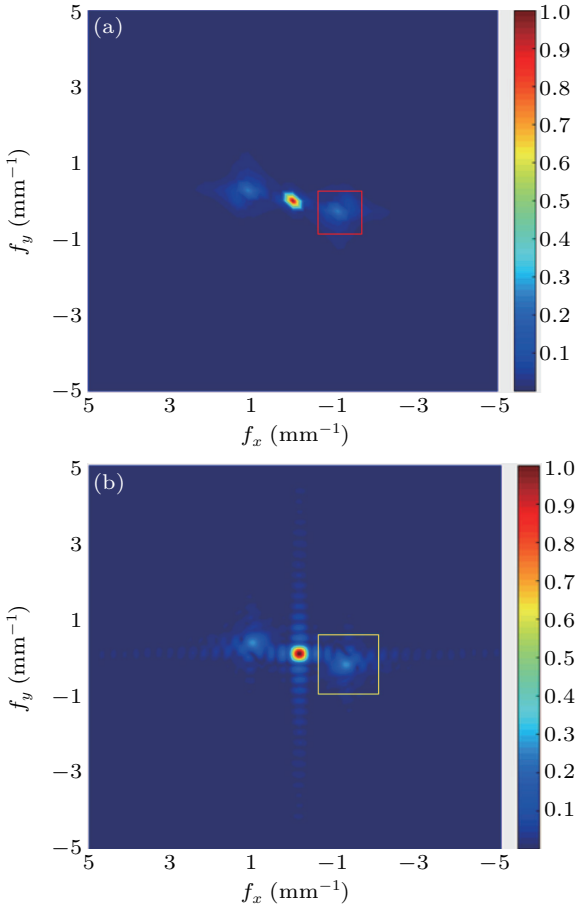


Fig. 15. The selection of the first-order calculation window for different methods. (a) FFT (red window); (b) the proposed method (yellow window).

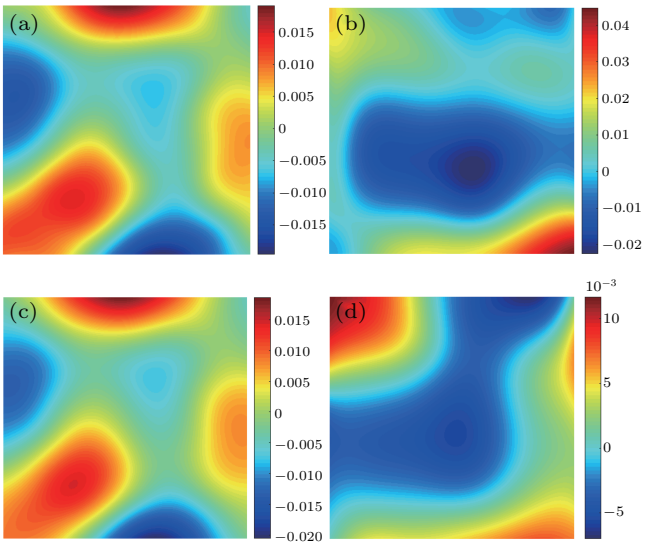


Fig. 16. The comparison of retrieved results based on FFT and the proposed method. (a) and (b) represent the result of FFT, and RMS $= 0.112\lambda$; (c) and (d) represent the result of the proposed method at the $\alpha = 4$, and RMS $= 0.035\lambda$.

In order to verify the repeatability of the proposed method, the measurement is performed 10 times under the same modulation phase. The residual RMS curve of the measurement result is shown in Fig. 17. It can be seen that the residual RMS fluctuates only a little, and the largest RMS is 0.035λ. The experimental results show that the proposed method has good repeatability.

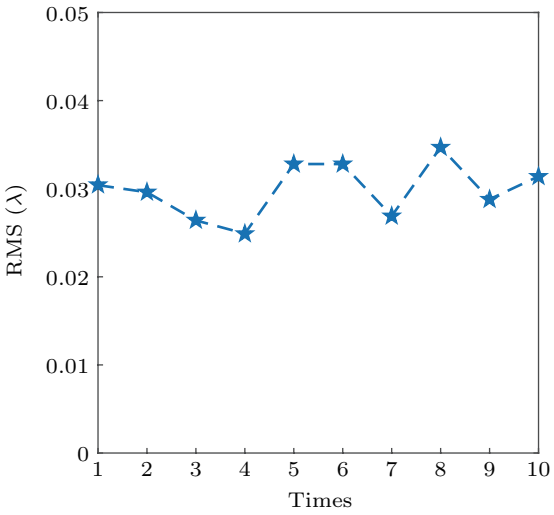


Fig. 17. The results of repeated measurements.

6. Conclusion

In conclusion, the broad-band phase-retrieval method based on CZT is proposed for the transient radial shearing interference, which has the advantages of determining the optimal carrier frequency and calculation window, and strengthens the ability of retrieving information. The coarse definition of the calculation window in traditional FFT results in a small bandwidth of the retrievable phase; the proposed method can be customized, which increases the bandwidth of phase retrieval. Through simulation, the residual RMS of the traditional FFT is 0.146λ, while the residual RMS of the proposed method in the paper is 0.037λ. In the experiment, the RMS values of the two methods are 0.112λ and 0.035λ respectively, and the experimental verification shows that the results are basically consistent with the simulation results, indicating that the retrieved accuracy of the CZT-based broad-band phase retrieval method is an order of magnitude higher than that of FFT. At the same time, the method has shown better robustness and repeatability. It can also be used in other types of spatial carrier frequency interference. For applications such as laser beam quality evaluation, the broad-band phase-retrieval method based on CZT provides a more effective means for the transient radial shearing interference, which can significantly improve the practicable value of the phase-retrieval algorithm.

References

[1] Gu N, Huang L, Yang Z, Luo Q and Rao C 2011 *Opt. Lett.* **36** 3693
[2] Dong L, Yang Y, Wang L and Zhuo Y 2007 *Appl. Opt.* **46** 8305
[3] Yang Y, Lu Y, Chen Y, Zhuo Y, Zhang X, Chen B and Qing X 2005 *SPIE Proc.* **5638** 200
[4] Zhang Q and Wu Z 2013 *Opt. Lasers Eng.* **51** 253
[5] Murty M and Shukla R 1973 *Appl. Opt.* **12** 2765

[6] Liu D, Yang Y, Weng J, Zhang X, Chen B and Qin X 2007 *Opt. Commun.* **275** 173
[7] Chen Y, Zeng S and Xu M 2018 *SPIE Proc.* **10815** 108151A
[8] Kohno T, Matsumoto D, Yazawa T and Uda Y 1997 *SPIE Proc.* **3173** 280
[9] Edwards C B, Lee P and Tatarakis M 1995 *SPIE Proc.* **2375** 254
[10] Pu H, Li D, Luo P and Zhang C 2020 *Opto-Electronic Engineering* **47** 190390 (in Chinese)
[11] Mochida S, Shinomura M, Hirakawa T, Fukuda T, Awatsuji Y Nishio K and Matoba O 2018 *SPIE Proc.* **10711** 1071114
[12] Debnath S K and Park Y K 2011 *Opt. Lett.* **36** 4677
[13] Toto-Arellano N I, Rodriguez-Zurita G, Meneses-Fabian C and Vázquez-Castillo J F 2009 *J. Opt. A: Pure Appl. Opt.* **11** 045704
[14] Rao K R, Kim D N and Hwang J J 2013 *Fast Fourier Transform: Algorithms & Applications* pp. 28–95
[15] Hariharan P and Sen D 1961 *IOP Science* **38** 428
[16] Wang Y, Da Z 2016 *Infrared and Laser Engineering* **45** 0317001
[17] Guo Y, Chen X, Zhang T 2014 *Opt. Lasers Eng.* **63** 25
[18] Juarez-Salazar R, Guerrero-Sanchez F and Robledo-Sanchez C 2015 *Appl. Opt.* **54** 5364
[19] Li Y, Guo J, Liu L, Wang T and Shao J 2014 *J. Mod. Optic.* **61** 1519
[20] Pan A, Zhou M, Zhang Y, Min J, Lei M and Yao B 2018 *Opt. Commun.* **430** 73
[21] Nascov V and Logofătu P C 2009 *Appl. Opt.* **48** 4310
[22] Ghiglia D C and Pritt M D 1998 *Two-Dimensional Phase Unwrapping: Theory, Algorithms, and Software* p. 500